

Numerical Simulation of Flow in a Solid Rocket Motor: Combustion Coupled with Regressive Boundary

Mehmet Özer Havlucu

Department of Mechanical Engineering
Istanbul Technical University
Istanbul, Turkey
havlucum@itu.edu.tr

Kadir Kırkköprü

Department of Mechanical Engineering
Istanbul Technical University
Istanbul, Turkey

Abstract—A computational model is developed for the simulation of internal reactive fluid flow in a solid rocket motor with propellant burning surface regression. The model focuses on a 2D reactive flow in an end burning lab-scale motor. Chemical reaction equations with finite rate chemistry are combined with gas dynamics, and complete conservation equations of mass, momentum, energy and species are solved. Two different chemical systems, hydrogen and propane combustion processes, are studied. The regressive boundary in the combustion chamber is treated using remeshing techniques. The effect of propellant regression on gas mixture velocity and temperature distribution in the flame zone is examined. Thrust values with varying inlet temperatures are compared for both combustion models.

Keywords—solid rocket motor; combustion; solid fuel regression; remeshing

I. INTRODUCTION

Conceptually, solid rocket motors (SRMs) are simple devices converting chemical-thermal energy into kinetic energy. SRMs are reaction engines in which propellant goes through chemical reactions inside the combustion chamber and produces hot gases. The ejection of these hot gases from the nozzle with high speed produces thrust and thus propels the rocket forward. Therefore, the control of SRM requires thorough understanding of combustion coupled gas flow associated with moving internal boundary, which is an extremely complicated phenomenon [1].

First, gas flow in chamber was studied with cold-flow approach where inert gases are injected into the chamber. Analytic expressions for velocity distributions were obtained for incompressible laminar flow [2, 3]. Dunlap and his co-workers experimentally characterized cold flow field that develops along a cylindrical port of rocket chamber and studied injection driven flow with injection Mach numbers 0.0018 and 0.0036 to achieve centerline Mach numbers of 0.14 and 0.27, respectively [4]. Similarly, Traineau and his co-workers [5] performed cold flow simulation tests of

a nozzleless solid rocket motor using porous walled 2-D duct and studied pressure and Mach number variations along the chamber. Later, the compressibility effect is studied analytically by Balakrishnan and his co-workers [6].

In solid propellant rocket motors the reaction zone is very thin, in the order of few millimeters and complicated to be described mathematically [7]. Modeling of this thin layer requires challenging computational effort. Therefore, researchers are formerly encouraged to model the flow in the chamber as cold flow induced by mass inflow from side surfaces mimicking the propellant surface. For instance, 2D Navier-Stokes computations were performed on a simple cylindrical motor with models representing propellant combustion response [8]. Euler and Navier-Stokes equations were solved in a 2D test case representing SRM using artificial viscosity terms by Lupoglazoff and Vuillot [9]. Alavilli and his co-workers used a Navier-Stokes solver and developed an efficient conductive heat transfer model by combining gas flow and heat transfer to the propellant [10]. Uygun and Kırkköprü [11] studied and simulated the flow in SRM chamber considering two-dimensional unsteady cold flow with regressing propellant boundary. Similarly, Terzic and his co-workers [12] conducted numerical simulation of pressure dependent burning surface regression to predict internal ballistics performance of solid propellant rocket motors.

Reactive fluid flow and understanding its characteristics is an important aspect of SRM. As computational powers increased, researchers started to combine the cold flow with reaction to reveal reactive fluid flow. Numerical analysis of combustion dynamics of homogenous SRM with stagnant wall boundaries was studied by Apte and Yang [13]. Similarly, El-Askary and his co-workers described combustion process in a SRM combustion chamber considering 2D, multi component reactants with turbulent compressible flow [14]. Chu and his co-workers [15], studied unsteady state response of a laminar flame to acoustic waves in two dimensional combustion chamber with surface mass injection and coupled flow dynamics with vortico-acoustic waves.

Yumusak [16] developed a computational method to assess internal flow of two dimensional propulsion system using Euler equations. The author further developed a design tool for optimized nozzle geometry using viscous flow for SRM [17].

As trust in SRM is generated through chemical reaction and expansion and acceleration of chemical products by passage through a nozzle at the rear of the rocket, the design and the performance of SRMs depends heavily on combustion processes and fluid flow. The other key factor contributing to the SRMs design and performance is regressive burning surface [18]. As combustion takes place, combustion chamber geometry is no longer constant due to the regression of the solid fuel as it converts into the gaseous mixture. Burning area changes results in changes in flow field inside the chamber of rocket motors. Thus, in the present work, a computational method is developed to simulate chemical reaction coupled with gas flow inside combustion chamber of SRM with regressive boundary. The model was applied to compressible two-dimensional channel flow. Finite volume discretization (approach) is utilized and Euler equations with finite rate chemistry are solved with mass, energy and species equations. The reactive gas flow model is validated against the study by Yumusak [16]. SRMs thrust comparisons are presented for different inlet temperatures combined with constant regression velocity.

This study describes firstly the configuration of the combustion model where the chemical combustion process with gas flow takes places. Thereafter, the mathematical model and governing equations of the reacting flow under considered geometry is explained. Chemical reactions, numerical model and initial conditions are introduced. Reacting flow in a combustion channel with no regressive boundary is verified. The numerical model is further combined with regressive burning boundary and different combustion processes, H_2 and C_3H_8 based combustion reactions are studied. Results and discussion of these models and effect of regressive boundary on temperature and velocity profiles are examined in detail.

II. COMPUTATIONAL MODEL

Figure 1 illustrates a schematic combustion chamber of SRM. The model is a 2-D end-burning lab-scale motor which has a chamber length of 170 mm. The half height is 45 mm. It is connected downstream to a converging-diverging nozzle with a half throat height of 16.77 mm and radius of curvature of 30 mm. The flow space length including the nozzle is 270 mm. The gaseous fuel premixed with O_2 is injected at low Mach number subsonic conditions from the head-end surface perpendicular to the main stream. Two different gaseous fuels considered in this study are H_2 and C_3H_8 .

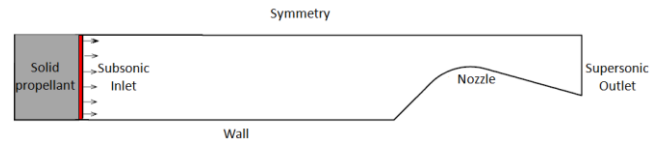


Fig. 1. Geometric representation of lab-scale motor.

Boundaries are a symmetric upper boundary, an impermeable lower wall and the burning head end. The gaseous mixture leaves the combustion chamber through a nozzle at supersonic conditions. On the head-end, propellant surface degrades, as it burns. Boundary regression to the left is taken into account in calculations in Section VIII.

III. GOVERNING EQUATIONS

The model of the two-dimensional reactive flow is based on conservation equations of mass, momentum, energy, and species concentrations for all multicomponents of the chemically reacting system. For a system with N number of species, the governing equations of time dependent Euler equations take the generic vector form.

$$\frac{\partial Q}{\partial t} + \frac{\partial F}{\partial x} + \frac{\partial G}{\partial y} = H \quad (1)$$

where Q, F, G and H are

$$Q = \begin{bmatrix} \rho \\ \rho u \\ \rho v \\ \rho E \\ \rho Y_1 \\ \rho Y_2 \\ \dots \\ \rho Y_{N-1} \end{bmatrix} \quad F = \begin{bmatrix} \rho u \\ \rho u^2 + p \\ \rho uv \\ [\rho E + p]u - \rho \sum_{i=1}^N h_i D_i \frac{\partial Y_i}{\partial x} - k \frac{\partial T}{\partial x} \\ \rho Y_1 u - \rho D_1 \frac{\partial Y_1}{\partial x} \\ \rho Y_2 u - \rho D_2 \frac{\partial Y_2}{\partial x} \\ \dots \\ \rho Y_{N-1} u - \rho D_{N-1} \frac{\partial Y_{N-1}}{\partial x} \end{bmatrix}$$

and

$$G = \begin{bmatrix} \rho v \\ \rho uv \\ \rho v^2 + p \\ [\rho E + p]v - \rho \sum_{i=1}^N h_i D_i \frac{\partial Y_i}{\partial y} - k \frac{\partial T}{\partial y} \\ \rho Y_1 v - \rho D_1 \frac{\partial Y_1}{\partial y} \\ \rho Y_2 v - \rho D_2 \frac{\partial Y_2}{\partial y} \\ \dots \\ \rho Y_{N-1} v - \rho D_{N-1} \frac{\partial Y_{N-1}}{\partial y} \end{bmatrix} \quad H = \begin{bmatrix} 0 \\ 0 \\ 0 \\ q \\ s_1 \\ s_2 \\ \dots \\ s_{N-1} \end{bmatrix}$$

Here, ρ , u , v , p , E , Y_N represent the total density, x velocity, y velocity, pressure, the total energy and the mass fraction of the N^{th} species, respectively. h_i is the

mass enthalpy for i^{th} species, D_i is the diffusion coefficient and q is the heat of the chemical reaction. Source term, s_N , includes contributions from chemical reactions taking place inside the combustion chamber and it represents the rate of change of every species due to the chemical reaction.

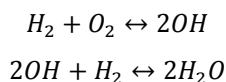
It is assumed that thermodynamic properties are thermally perfect. Within the domain the specific heat of the species are taken as a function of temperature and perfect gas mixing law is used for the mixture specific heat. Additionally, gravitational force and radiative heat transfer are neglected. The flow is assumed to be laminar everywhere in the domain.

IV. BOUNDARY CONDITIONS

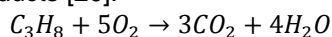
There are four boundary conditions for the lab-scale model. The left side of the model which is the end-burning part is taken as a subsonic inlet. The mass flux at this injecting boundary is $11.39 \text{ kg/m}^2\text{s}$ and the injection temperature is 3387 K as in the study by Yumusak [16]. The fuel-air equivalence ratio is 0.3. The upper part has a symmetry boundary condition. The velocity in y-direction is set to be zero at this boundary. The lower solid impermeable boundary and the nozzle wall are adiabatic. The gaseous mixture leaves the nozzle at supersonic conditions. For supersonic outflow the flow properties are calculated from the interior points.

V. CHEMICAL MODEL

Despite the recent developments in computational resources, thorough consideration of all physical and chemical processes in SRM and modeling of those are still challenging. A simplified reaction mechanism can therefore be considered to describe the combustion process. In this study, a chemical model based on the combustion of hydrogen gas with air is considered at first. Hydrogen combustion process is assumed to follow a two step model, where in the first step hydrogen reacts with oxygen to form hydroxide and in the latter hydroxide combines with hydrogen to compose gaseous water molecule. This reaction mechanism has been well established and captures information about the major chemical kinetic pathways. It can be represented by the following steps [19].



The effect of the chemical model on combustion coupled flow is also considered in the present study. The combustion of propane is assumed to follow a one step reaction, which yields carbon dioxide and water vapor as products [20].



VI. NUMERICAL MODEL

The governing equations coupled with the chemical reactions are solved using the commercial software ANSYS Fluent 15.0 [20]. The combustion is treated using finite rate chemistry model. Spatial discretization is obtained using second order upwind differencing scheme and temporal discretization is achieved using first order implicit method. The geometry shown in Figure 1 is a two dimensional channel with symmetry condition.

Temperature and species mass fractions vary very rapidly within a very thin zone adjacent to the boundary mimicking the propellant surface. Thus, to better capture these rapid variations of flow properties within this thin regime, cells are highly clustered in the neighborhood of the end burning part of the motor as were done by others [10,11,15]. Figure 2 illustrates the computational grids near the head end of the computational domain. The smallest cell which is next to the transpiring left-hand wall is taken as 0.015 mm thick. The dimensions of the subsequent ones in axial direction are set to be 1.05 times the previous one (The growth factor is 1.05). This sizing strategy in gridding holds till 30 mm away from the head end boundary. Beyond this distance onwards, the sizes of the grids are taken uniform. 50 uniform and 224 non-uniform grids are used in the vertical and horizontal directions, respectively. Under-relaxation factor of 0.7 within each time step is used for pressure, momentum and temperature for numerical stability.

The convergence residuals for continuity, velocity, energy, and mass fractions of the species are set to be 10^{-3} for every iteration in each time step for unsteady calculations. When the steady state results are reached, the absolute residual of energy and velocity are 4×10^{-5} and 8×10^{-5} , respectively.

Steady state calculations are achieved by setting the temperature at all grid points equal to the adiabatic flame temperature of the combustion model, initially. Accordingly, velocity field and species mass fractions in the domain are taken equal to the inlet velocity and species mass fractions at the end burning boundary. The numerical solutions diverged while using the Euler equations. Therefore, first the flow field is solved using the Navier-Stokes equations, then these solutions are taken as the initial conditions for the Euler type model. Non-regressive and regressive boundary models will be explained in the following part. Non-regressive boundary model results are verified with the inviscid non-regressive study of Yumusak [16].



Fig. 2. Grid structure next to the end burning boundary.

VII. NON-REGRESSIVE BOUNDARY MODEL

The hydrogen and oxygen gases with equivalence ratio of 0.3 emanate from the stationary head end with mass flux of $11.39 \text{ kg/m}^2\text{s}$ at 3387 K as in the study by Yumusak [16]. Remaining boundaries are treated as explained previously. The final steady state solutions are obtained using the time marching technique offered by the software Fluent 15.0 [20].

The chemical reaction of the fuel air mixture in a very thin flame zone close to solid propellant surface is shown in Figure 3. Within this flame zone, the variations of flow properties such as temperature and species mass fractions are very rapid. The temperature increases from the feeding boundary temperature of 3387 K to 3807 K in a distance less than a millimeter. The flow characteristics within this region are captured using grids that are highly clustered near the end burning part of the motor. Figure 3 also compares mass fractions of H_2 , O_2 and H_2O species along the axis of the combustion chamber. H_2 and O_2 mass fractions decrease from 0.0083 and 0.22 corresponding the equivalence ratio 0.3 to 0.0001 and 0.155, respectively. The mass fraction of the product, H_2O , increases from 0 to 0.07.

Figure 4 represents the temperature contours for both present and Yumusak's study [16]. With an inlet temperature of 3387 K the temperature of the mixture increases to 3807 K. The thin flame zone is not observed in this figure, since this zone is very small compared to the size of the combustion chamber. After the chemical reaction takes place, the maximum

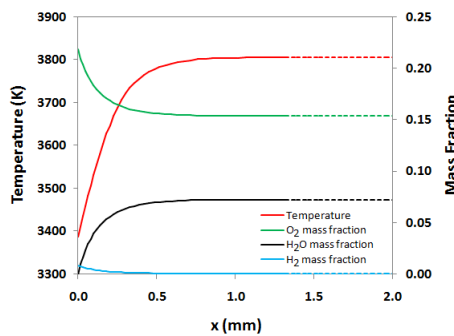


Fig. 3. Temperature and mass fractions along x-axis from the burning end.

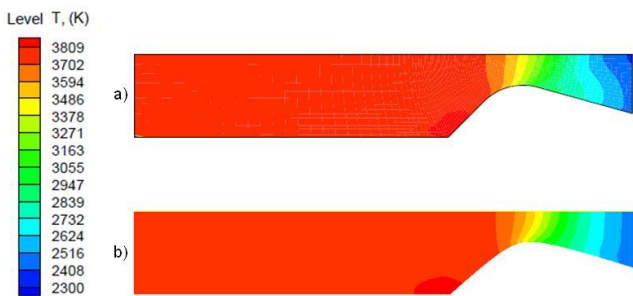


Fig. 4. Comparison of temperature contours a) Contour map from the work of Yumusak [16] b) Contour map from the current study.

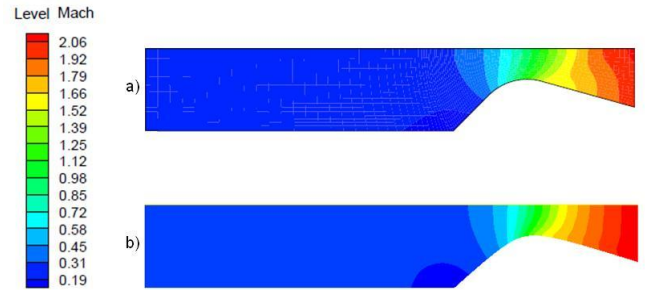


Fig. 5. Comparison of Mach number contours a) Contour map from the work of Yumusak [16] b) Contour map from the current study.

temperature is achieved 3807 K in the present study which is very close to the value of 3804 K in the work of Yumusak [16]. All the way down to the inlet of the nozzle, the temperature remains nearly constant since the chamber wall is adiabatic. Close by the throat of the nozzle, the temperature starts to decrease. The temperature contours match for both studies except in a small section of the diverging part of the nozzle possibly due to different numerical treatments. Temperature takes value around 2400 K at the exit of the motor for both studies.

The comparison of Mach number contours in the present study with those obtained by Yumusak [16] is shown in Figure 5. The Mach number remains almost constant through the rectangular part of the channel as does the temperature. As the flow enters the nozzle the Mach number starts to increase and reaches the sonic value at the nozzle throat for both studies and contours look similar except in the small section of the diverging part of the nozzle as do the temperature contours. Mach number takes the maximum value of 2.10 at the exit of the nozzle in the current study whereas it takes 2.06 in the referenced study.

VIII. REGRESSIVE BOUNDARY MODEL

SRM has a variable internal geometry due to the transformation of the solid propellant to reactant and oxidizer to form combustion products. This variation in geometry with changing combustion area in time results in change of pressure and thrust and thus causing a change in SRM performance.

Once steady state solutions are obtained and validated without regression on the end burning boundary, more complex SRM modeling is imposed through numerical model. In this part, the same geometry as that without regression is considered. Boundary conditions are taken same as the previous case except the inlet temperature and the equivalence ratio on the end boundary. In this case, two different inlet temperatures, 350 K and 800 K, are considered with equivalence ratio of 0.7. First, non-regressive model with chemical reaction model is solved until steady state results are obtained for the prescribed inlet temperatures. Then, these steady results are set as initial conditions for the unsteady numerical

calculations with regressive boundary, as done by others [11].

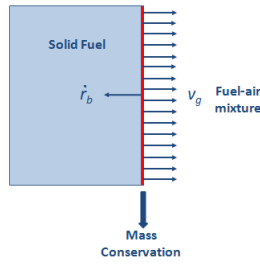


Fig. 6. Surface regression model [25].

Surface regression is modeled with a layer between solid propellant grain and the gases which are the fuel-air mixture as shown in Figure 6. The left part is solid fuel with oxidizer. The red zone is the layer where solid fuel is vaporized to form reactant and oxidizer gases. Therefore, it is assumed that the reaction starts at the interface between the red zone and the chamber. As combustion occurs, the amount of the solid fuel decreases and the boundary regresses to the left. Displacement of the burning surface is considered as parallel layers normal to burning surface of the propellant grain [12]. The movement of this boundary is governed by the burning rate \dot{r}_b . In the literature, several formulations are offered to predict the burning rate of an energetic solid propellant [7,18,21-24]. One of the well-known formulations is the APN model, which approximates the burning rate as solely dependent on the mean local pressure within the combustion chamber [18]. The pressure dependency of the burning rate, is however, not considered in this study; instead a constant burning rate is assumed.

As surface regresses with burning rate, \dot{r}_b , the reactant and oxidizer gases leave the burning surface in opposite direction with the velocity V_g . Since the propellant density ρ_p is much higher than the density of the gaseous reactant and oxidizer mixture ρ_g , the velocity of this mixture is significantly greater than the burning rate. Thus, conservation of mass is approximately [25]:

$$\rho_p \dot{r}_b \approx \rho_g V_g \quad (2)$$

Here the velocity V_g or the mass flux $\rho_g V_g$ can be determined through Equation (2), because the density of the propellant and the burning rate of the regressing boundary are known. The density of the propellant is taken 1633 kg/m^3 [11] and the corresponding burning rate is $6.97 \times 10^{-3} \text{ m/s}$.

To numerically model the regression of the burning surface boundary, user-defined functions (UDF) are customized using C++ [26] and implemented in ANSYS Fluent 15.0 [20]. Displacement of the boundary is considered only in x direction. With this assumption, the end burning boundary regression is calculated using the below expression:

$$x_{new} = x_{old} - \dot{r}_b \Delta t$$

x_{new} is the calculated new x-coordinate of the boundary at the end of the time step Δt . First order implicit method is used for the temporal discretization. x_{old} is the x-coordinate of the boundary in the previous time step. \dot{r}_b is the constant burning rate. At the end of every time step, the location of the moving boundary is calculated and updated. New rectangular grids are added to the left of the computational domain for every regression distance of 0.03 mm. The initial thickness of the propellant 100 mm is added to the total length of 270 mm. Given the constant burning rate of $6.97 \times 10^{-3} \text{ m/s}$, the propellant is consumed in 14.35 seconds. During the unsteady combustion process with regressive boundary new vertical uniform grid lines are added in the horizontal direction.

Numerical simulation of regression of the end burning boundary is examined in a 2D transient, laminar, reactive flow model. Using this simulated model, effects of regressive boundary on temperature profile, velocity profile in the axial direction for H_2 combustion and SRM thrust curves for both H_2 and C_3H_8 chemical models are studied.

Figure 7 illustrates the temperature profiles both for no regression and 1 mm regression of the solid fuel boundary with inlet temperature of 350 K. Considering an equivalence ratio of 0.7 for H_2 combustion, the temperature reaches a maximum value of 1918 K in both models indicating that the chemistry is not affected from the boundary regression.

Grid independency of the simulation is studied using various grid sizes. Figure 8 shows the temperature profiles both for no regression and 1 mm regression of the solid fuel boundary for grid sizes of 0.03 mm, 0.015 mm and 0.0075 mm with inlet temperature of 350 K. It is observed that, considered grid sizes result in the same temperature profiles for both models, no regression and with regression. Thus for computational cost, minimum grid size of 0.03 mm is used in the present study.

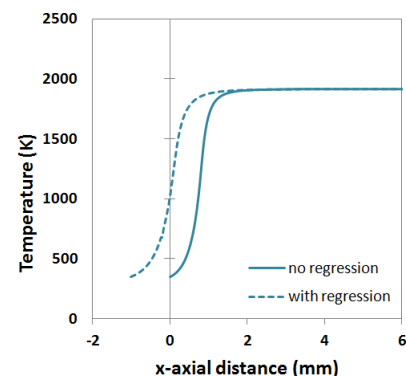


Fig. 7. Temperature profiles from the burning end with regression to $x=1 \text{ mm}$ corresponding $t=143 \text{ ms}$ and with no regression and for inlet temperature of 350K.

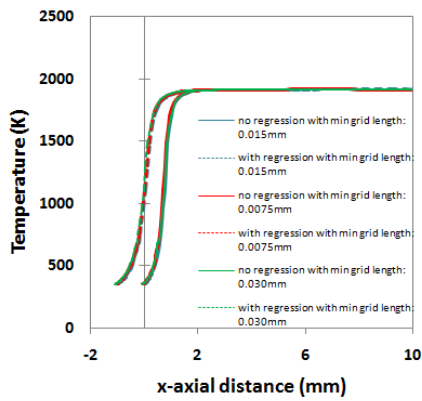


Fig. 8. Temperature profiles from the burning end with regression to $x=1$ mm corresponding $t=143$ ms and with no regression for minimum grid size of 0.03 mm, 0.015 mm and 0.0075 mm for inlet temperature of 350 K.

Temperature profile at a higher inlet temperature, 800 K, was also studied. As it is seen from Figure 9, introducing moving boundary does not affect the maximum temperature, in both (regression and no regression) models it reaches a maximum value of 2014 K. Compared to the temperature profiles with an inlet temperature of 350 K in Figure 10, those obtained at 800 K show a steeper trend.

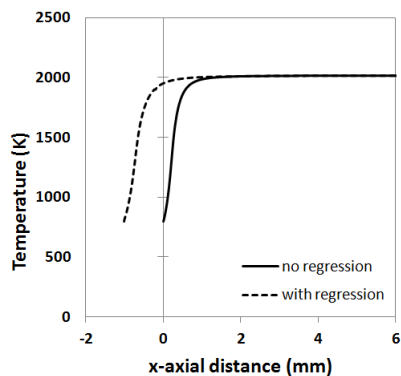


Fig. 9. Temperature profiles from the burning end with regression to $x=1$ mm corresponding $t=143$ ms and with no regression for inlet temperature of 800 K.

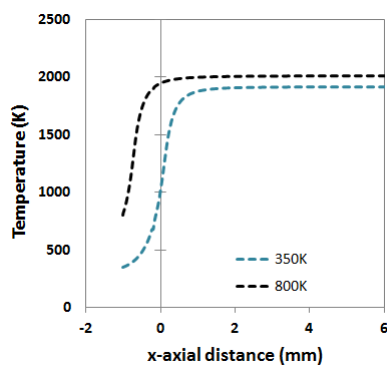


Fig. 10. Temperature profiles from the burning end with regression to $x=1$ mm corresponding $t=143$ ms and for inlet temperatures of 350 K and 800 K.

The comparison of temperature variation in the chamber for H_2 and C_3H_8 for the inlet temperature of 350 K at the same mass flux of $11.39 \text{ kg/m}^2\text{s}$ is shown in Figure 11. In the reaction zone, the temperature

increases to 1918 K for the hydrogen combustion and to 1792 K for the propane combustion, respectively.

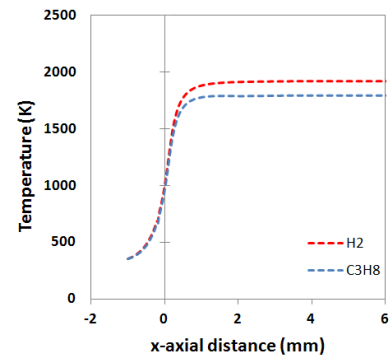


Fig. 11. Temperature profiles from the burning end with regression to $x=1$ mm corresponding $t=143$ ms for H_2 and C_3H_8 combustion.

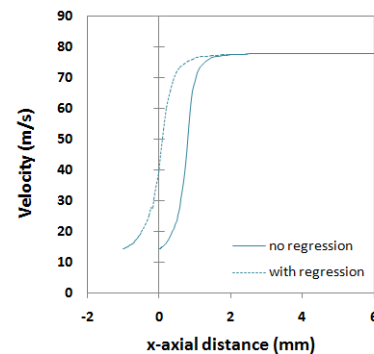


Fig. 12. Velocity of gas mixture versus distance from the burning end with regression to $x=1$ mm corresponding $t=143$ ms and with no regression for inlet temperature of 350 K.

The velocity distribution along the x-axis with inlet temperature of 350 K and equivalence ratio of 0.7 with regression and no regression is presented in Figure 12. The temperature increases rapidly in the 2 mm thin reaction zone as shown in the previous figures. The mixture of combustion gases expands and the velocity of the gaseous mixture increases from 14.23 m/s to 77.76 m/s in this thin zone. The corresponding Mach number is 0.0386 for the inlet velocity and it reaches the value of 0.09 at the end of the reactive flame zone.

IX. THRUST CURVES

Effects of regressive boundary on SRM thrust curves are also investigated. Thrust is known as the force that propels SRM which is due to the effect of pressure exerted on the walls of the combustion chamber.

The pressure distribution within the combustion chamber is asymmetric, inside the chamber only minimal pressure variations are observed whereas on the downstream, near the nozzle, it decreases. The gas pressure on the downstream and the force associated with that is not compensated by the outside. As a result of the internal and external pressure differences and pressure exerted on the walls

of the chamber, thrust occurs and propels chamber forward.

Considering the forces due to the pressures exerted on the walls of the chamber by the combustion gases and the surrounding atmosphere and taking the cross sectional area of the exit on downstream and using that as the boundary between the inner and outer mathematically, thrust, F , is defined as:

$$F = \dot{m}V_e + (p_e - p_0)A_e$$

where \dot{m} is the mass flow rate, V_e is the exit velocity of the gaseous mixture and p_e and p_0 are the exhaust gase pressure and ambient pressure, respectively. A_e is defined as the cross sectional area at the exit of at the nozzle. The first term on the right-hand side of the equation is the contribution due to flow and the second term on the right-hand side is called pressure thrust which could only have negative value or could be equal to zero for a nozzle with an optimum expansion ratio ($p_e = p_0$). Under the optimal design criteria, thrust achieves its highest value and thus SRM performance achieves its maximum level.

Within the explained lab-scale SRM model, as the gaseous combustion products leave the nozzle with a Mach number greater than 1 (at supersonic conditions) significant thrust occurs propelling the chamber forward. Figure 12 illustrates the time dependent thrust profiles that are obtained for hydrogen combustion model at varying inlet temperatures.

In Figure 13, at each inlet temperature, the thrust curve starts from a particular value since the steady results are set as the initial conditions for regressive boundary unsteady model. Thrust profiles remain almost constant throughout the first second. After the first second, a gradual decrease starts in the thrust value. When the propellant is consumed totally, corresponding time $t=14.35$ seconds, the decrease in thrust is about 10 %. These trends can be explained by considering the regressive boundary. The lab scale motor is 270 mm long including the nozzle. A solid fuel thickness of 100 mm is added to it. During the regression, the volume change of the chamber is about 44 %. The increase in the chamber volume results in pressure decrease. Thus, thrust decreases in time. Figure 13 also shows that increase in inlet temperature results in an increase in thrust.

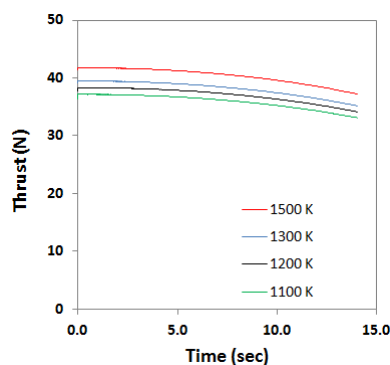


Fig. 13. Thrust profiles for H_2 combustion.

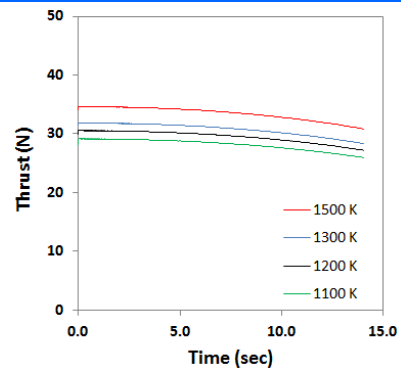


Fig. 14. Thrust profiles for C_3H_8 combustion.

Similarly, thrust profiles for propane combustion model are provided for different inlet temperatures in Figure 14. Increased inlet temperatures increase the thrust and the thrust versus time behaves as that for H_2 combustion.

Hydrogen and propane combustion models are also compared for the inlet temperatures of 350 K and 800 K in Figure 15 and Figure 16, respectively. For the inlet temperature of 350 K in Figure 15, maximum thrust is 26.2 N for hydrogen combustion and 19.6 N for propane combustion, respectively. These values decrease to 23.1 N for hydrogen and 17.5 N for propane combustion when the solid propellant is entirely consumed at time $t=14.35$ seconds.

As seen in Figure 16, maximum thrusts are 32.9 N and 24.7 N for hydrogen and propane combustions with the inlet temperature of 800 K. These values decrease to 29.2 N and 22.8 N for hydrogen and propane combustions, respectively.

Figure 15 and Figure 16 show that the thrust value of the hydrogen combustion model is higher than that of the propane combustion model for the same mass influx and the same inlet temperature on the head end burning regressive boundary.

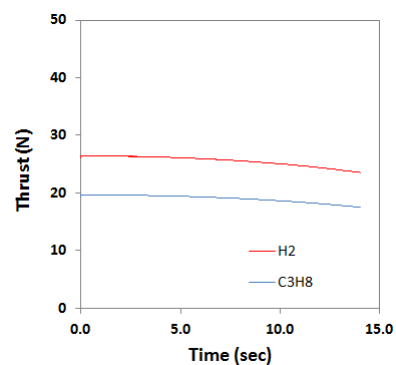


Fig. 15. Thrust profiles for H_2 and C_3H_8 combustion, inlet temperature of 350 K for mass flux of $11.39 \text{ kg/m}^2\text{s}$.

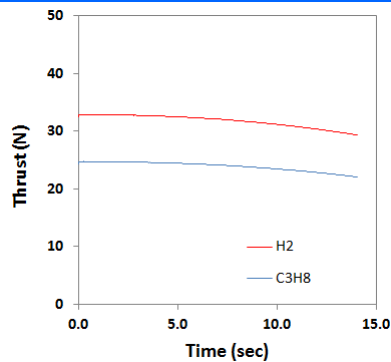


Fig. 16. Thrust profiles for H_2 and C_3H_8 combustion, inlet temperature of 800 K for mass flux of $11.39 \text{ kg/m}^2\text{s}$.

X. CONCLUSIONS

This study has focused on the relevance between flow characteristics and combustion dynamics in solid rocket motor chambers. A computational method was developed which simulates gas flow coupled with chemical reaction inside combustion chamber with regressive boundary including remeshing technique. Complete conservation equations representing reacting flow with finite rate chemistry were solved. Results of the developed numerical model were verified against published study with non-regressive boundary. The model was further developed to account for regressing boundary of burning solid fuel. To serve for this purpose, an unsteady state simulation including constant regression rate model for the solid fuel boundary was coupled with two dimensional reactive flow. An end-burning lab-scale motor with regressive burning solid surface is studied for two different chemically reactive systems, hydrogen and propane combustion processes. Results of the coupled simulation of the reactive fluid flow with propellant burning surface regression demonstrate that about 44 % of the chamber volume increase causes about 10 % decrease in thrust. Increasing the inlet temperature also increases thrust value. Comparing the two different reactive systems leads to the fact that hydrogen combustion model results in higher thrust under same inlet conditions.

REFERENCES

[1] M. A. Willcox, M. Q. Brewster, K. C. Tang, D. S. Stewart and I. Kuznetsov, "Solid rocket motor internal ballistics simulation using three-dimensional grain burnback", *J. Propul. Power*, 2007, Vol. 23 (3), pp. 575–584.

[2] G. I. Taylor, "Fluid flow regions bounded by porous surfaces", *Proceedings of the Royal Society of London, Series 234A*, Vol. 11199, pp. 456-475, 1956.

[3] F. E. C. Culick, "Rotational axisymmetric mean flow and damping of acoustic waves in a solid propellant rocket", *AIAA Journal*, Vol. 4, pp.1462-1464, 1966.

[4] R. Dunlap, A. M. Blackner, R. C. Waugh, R. S. Brown, and P. G. Willoughby, "Internal flow field studies in a simulated cylindrical port rocket chamber", *J. Propul. Power*, Vol. 6, pp. 690-704, 1990.

[5] J. C. Traineau, P. Hervat, and P. Kuentzmann, "Cold-Flow simulation of a two-dimensional nozzleless solid rocket motor", *AIAA Paper*, 86-1447, 1986.

[6] G. Balakrishnan, A. Linan, and F. A. Williams, "Rotational inviscid flow in laterally burning solid-propellant rocket motors", *J. Propul. Power*, Vol. 8, pp. 1167–1176, 1992.

[7] A.M. Hegab, H.H. Sait, A. Hussain, A.S., Said, "Numerical modeling for the combustion of simulated solid rocket motor propellant", *Computers & Fluids*, Vol. 89, pp. 29-37, 2014.

[8] F. Vuillot, T. Basset, J. Dupays, E. Daniel and N. Lupoglazoff, "2D Navier-Stokes stability computations for solid rocket motors: rotational, combustion and two-phase flow effects", *AIAA*, Vol. 3326, pp. 1-11, 1997.

[9] N. Lupoglazoff, and F. Vuillot, "2D numerical simulation of vortex shedding phenomenon in 2D test case solid rocket motors", *AIAA*, Vol. 0776, pp. 1-9, 1992.

[10] P. Alavilli, J. Buckmaster, T. L. Jackson, and M. Short, "Ignition-transient modeling for solid propellant rocket motors", *AIAA*, Vol. 3567, pp. 1-9, 2000.

[11] M. Uygun, K. Kirkkopru, "Numerical simulation of unsteady flows in solid rocket motors with dual time stepping", *ITU Journal/d: Engineering*, Vol. 8(2), pp. 41-52, 2009.

[12] J. Terzic, B. Zecevic, S. Serdarevic-Kadic, and A. Catovic, "Numerical simulation of internal ballistics parameters of solid propellant rocket motors", 15th Seminar "New Trends in Research of Energetic Materials", University of Pardubice, Part II, pp. 881-892, 2012.

[13] S. Apte, and V. Yang, "Unsteady flow evolution and combustion dynamics of homogenous solid propellant in a rocket motor", *Combustion and Flame*, Vol. 131 (1-2), pp.110-131, 2002.

[14] W. A. El-Askary, S. A. Wilson, and A. Hegab, "Simulation of reactive fluid flow in a solid rocket motor combustion-chamber with/without nozzle", *CMES*, Vol. 76 (4), pp. 235-266, 2011.

[15] W. W. Chu, V. Yang, J. Majdalani, "Premixed flame response to acoustic waves in a porous-walled chamber with surface mass injection", *Combustion and Flame*, Vol. 133, pp. 359-370, 2003.

[16] M. Yumusak, "Non-reacting and reacting flow analysis in propulsion systems", Ph.D. Dissertation, The Middle East Technical University at Ankara, 2000.

[17] M. Yumusak, "Analysis and design optimization of solid rocket motors in viscous flows", *Computers and Fluids*, Vol. 75, pp. 22-34, 2013.

[18] Q. Li, G. He, P. Liu, and J. Li, "Coupled simulation of fluid flow and propellant burning surface regression in a solid rocket motor", *Computers and Fluids*, Vol. 93, pp.146-152, 2014.

[19] R. C. Rogers and W. Chinitz, "Using a global hydrogen-air combustion model in turbulent reacting flow calculations", *AIAA Journal*, Vol 21. No.4, pp. 586-592, 1982.

[20] ANSYS/Fluent, Software Package, Ver. 15.0, ANSYS, Canonsburg, PA, 2013.

[21] D. Greatrix, "Numerical evaluation of the use of aluminum particles for enhancing solid rocket motor combustion stability", *Energies*, Vol. 8, pp. 1195-1215, 2015.

[22] J. Montesano, K. Behdinan, D.R.Greatrix, Z. Fawaz, "Internal chamber modeling of a solid rocket motor: effects of coupled structural and acoustic oscillations on combustion", *Journal of Sound and Vibration*, Vol. 311, pp. 20-38, 2008.

[23] L. Wang, Z. Wu, H. Chi, C. Lui, H. Tao, Q.Wang, "Numerical and experimental study on the solid-fuel scramjet combustor", *Journal of Propulsion and Power*, Vol. 31, No.2, pp. 685-693, 2015.

[24] M. J. Ward, S. F. Son, and M. Q. Brewster, "Role of gas- and condensed-phase kinetics in burning rate control of energetic solids", *Combustion Theory and Modeling*, Vol. 2 (3), pp. 293–312, 1998.

[25] P. Kuentzmann, "Introduction to solid rocket propulsion", *Internal Aerodynamics in Solid Rocket Propulsion*, RTO Educational Notes EN-023, 2004.

[26] Microsoft Visual C++ 2010 Express, Software Package, Ver. 10.0.30319.1, 2010.